



A new torsion–rotation fitting program for molecules with a sixfold barrier: Application to the microwave spectrum of toluene

Vadim V. Ilyushin^{a,*}, Zbigniew Kisiel^b, Lech Pszczółkowski^b, Heinrich Mäder^c, Jon T. Hougen^d

^a Institute of Radio Astronomy of NASU, Chervonopraporna 4, 61002 Kharkov, Ukraine

^b Institute of Physics, Polish Academy of Sciences, Al. Lotników 32/46, 02-668 Warszawa, Poland

^c Institut für Physikalische Chemie, Christian-Albrechts-Universität zu Kiel, Olshausenstrasse 40, D-24098 Kiel, Germany

^d Optical Technology Division, National Institute of Standards and Technology, Gaithersburg, MD 20899-8441, USA

ARTICLE INFO

Article history:

Received 8 September 2009

Available online 29 October 2009

Keywords:

Toluene

Sixfold barrier

Internal rotation

Microwave spectrum

ABSTRACT

A new program is described for fitting rotation–torsion energy levels in molecules like toluene, in which the frame (C_6H_5) has C_{2v} symmetry and the methyl top has C_{3v} symmetry, i.e., for molecules where the internal rotation barrier is expanded in $\cos 6n\alpha$, where α is the internal rotation angle and $n = 1, 2, \dots$. The program is based on the theoretical framework developed by Sørensen and Pedersen in their application of the Longuet-Higgins permutation-inversion group G_{12} to the microwave spectrum of CH_3NO_2 . It is specifically designed for sixfold barrier molecules, and allows the user to select almost any symmetry-allowed torsion–rotation term for inclusion in the fitting Hamiltonian. This program leads to a very successful fit of transitions in the microwave spectrum of toluene characterized by $J \leq 30$, $K_a \leq 12$, and by the free-rotor quantum number $|m| \leq 3$. In these fits we included both published and rather extensive unpublished new measurements, for which fits using other torsion–rotation programs have not been very successful. The fit presented here uses 28 parameters to give an overall standard deviation of 7.4 kHz for 372 line frequencies, and results in a much improved value for the sixfold barrier for toluene, $V_6 = 13.832068(3) \text{ cal mol}^{-1}$.

© 2009 Elsevier Inc. All rights reserved.

1. Introduction

Most torsion–rotation fitting programs consider an expansion of the internal rotation barrier in $\cos 3n\alpha$, where α is the internal rotation angle and $n = 1, 2, \dots$, since such an expansion applies to the large class of molecules (like acetaldehyde) where the frame (CHO) has a plane of symmetry. In this paper we are concerned with molecules like toluene ($CH_3C_6H_5$), where the frame (C_6H_5) has C_{2v} symmetry, and the internal rotation barrier requires an expansion in $\cos 6n\alpha$.

Wilson, Lin, and Lide wrote an early paper [1] on the group theoretical considerations necessary for treating a molecule like CH_3BF_2 under the assumption of a rigid top and rigid frame, and came to the conclusion that a group of order 24 was appropriate. Nearly a decade later, Longuet-Higgins showed in his paper introducing the concept of permutation-inversion (PI) groups [2] that the correct group to use for this molecule is only of order 12 if the top and frame are allowed to undergo structural distortions during the internal rotation process. Sørensen and Pedersen used Longuet-Higgins' ideas to develop the theoretical expressions and computer program necessary for fitting the microwave spectrum

of CH_3NO_2 [3], and also confirmed the correctness of Longuet-Higgins' PI group G_{12} . Much later these ideas were used as the starting point for treatments of the infrared spectrum of CH_3CH_2 [4] and the $S_1 \leftarrow S_0$ electronic spectra of *p*-toluidene [5] and toluene [6,7].

In this paper we closely follow the approach of [3] to develop a new computer program for fitting torsion–rotation levels in molecules with a C_{3v} top and a C_{2v} frame (and therefore, a sixfold barrier), which allows the user to select essentially any symmetry-allowed torsion–rotation term for inclusion in the fitting Hamiltonian. We then apply this program to fit a relatively large data set containing old and new measurements of the microwave spectrum of toluene.

Toluene was chosen for the first application of the program since published and rather extensive unpublished data are available, and since fits of these data using other torsion–rotation programs available have not been very successful to date. Toluene is a prolate asymmetric top with $\kappa = -0.59$, and can be considered as a prototype for molecules with nearly free internal rotation of a methyl top with a sixfold barrier. The molecular structure, axis system, and atom numbering used in the present work are shown in Fig. 1.

The microwave spectrum of toluene was the subject of several previous investigations [8–11]. In the seminal study for this molecule, Rudolph et al. [8] assigned several low- J transitions in the

* Corresponding author. Fax: +380 57 706 1415.

E-mail address: ilyushin@rian.kharkov.ua (V.V. Ilyushin).

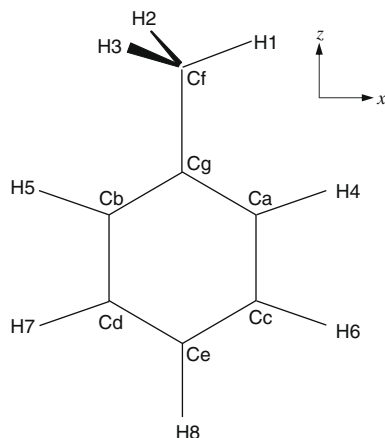


Fig. 1. Schematic illustration of the molecular structure of toluene, showing also the orientation of the axis system and the atom numbering used here. The coordinate system used to define the quantities α_i^0 in Eqs. (1)–(3) has its origin at C_g , so that the phenyl group has both an xz and a yz plane of symmetry. For positive V_6 and a sixfold potential of the form $(1/2)V_6(1 - \cos 6\alpha)$ the six equivalent minima resulting from internal rotation of the methyl group will correspond to coplanar orientation of the symmetry plane of the methyl group and the plane of the phenyl ring, with one methyl proton in the plane of the ring. Alternatively, for a sixfold potential of form $(1/2)V_6(1 + \cos 6\alpha)$ and again a positive V_6 , the equilibrium configuration will correspond to a perpendicular relative orientation of the methyl group symmetry plane and the ring plane, i.e., the equilibrium configuration will be that given by ab initio calculations and laser fluorescence experiments (see text).

$m = 0$ and $m = 3$ internal rotation states and measured the dipole moment. Most importantly they derived the much cited value $V_6 = 13.94 \pm 0.1$ cal/mol = $4.88(3)$ cm^{-1} for the sixfold internal rotation barrier. It should be noted, however, that their value was determined from analysis of a specific splitting affecting $m = 3$, $K = 1$ lines in the spectrum and was based on only two pairs of such lines identified in the spectrum. Their results were supplemented later by results for the deuterated [9] and the ^{13}C [9,10] isotopologues that allowed determination of the partial molecular geometry of toluene. In the most recent study of the rotational spectrum of toluene, the frequency ranges from 3.5 to 26.5 GHz and 160 to 330 GHz were investigated with four different spectrometers [11]. In that study an analysis of the ground state ($m = 0$) rotational spectrum of toluene was performed up to rather high values of $J \leq 92$. Previous microwave spectroscopic work on toluene has thus resulted in: a data set covering frequency ranges from 3.5 to 26.5 GHz and 160 to 330 GHz; a determination of the barrier height, partial geometry, and dipole moment; and a rather complete analysis of the rotational spectrum of the $m = 0$ internal rotation state.

The next natural step in studying the toluene spectrum was to try to analyze the rotational spectrum of $m \neq 0$ states ($m = 1, 2$, and 3), lines of which were clearly present in records obtained in the latest study [11]. Such an attempt was made by two of us (Z.K. and H.M.) using the XIAM [12] and SPFIT [13,14] programs. Although these programs allowed making assignments, which in the majority of cases were confirmed by further analysis using the new program described below, our $m \neq 0$ data could not be fit to experimental error using either of the two programs.

In the present study we have fit within experimental error a data set of 372 transitions with $J \leq 30$ belonging to $m = 0, 1, 2, 3$, and -3 states using 28 parameters, which gave an overall standard deviation of 7.4 kHz. Because of the considerable gap between 26.5 and 160 GHz in the frequency range covered to date, we decided to limit ourselves to $J \leq 30$ transitions, which constrained us to measurements made in the frequency range from 3.5 to 26.5 GHz. In the future we plan to supplement the presently available data set by measurements in the 50–150 GHz frequency range, which will

permit us to go smoothly in J assignments from the lower frequency range to higher frequencies. We note in passing that addition to the fit of high- J transitions already fitted in [11] for the $m = 0$ state does not pose any problem for the new program.

The rest of the paper is organized as follows. In Section 2 we review the group theoretical ideas necessary to take advantage of the symmetry of this molecule. In Section 3 we give a brief description of the structure of the computer fitting program. Experimental details and the data set treated here are described in Section 4. Section 5 discusses qualitative understanding of the torsion–rotation levels in toluene and Section 6 gives the fitting results and describes possible future work on this molecule.

2. Group theory

This section presents many of the ideas in [3], using in places, however, somewhat different language and/or a somewhat different level of detail.

2.1. Permutation-inversion group and coordinate transformations

At equilibrium, toluene belongs to the point group C_s , but as is now well known, when internal rotation of the methyl group against the phenyl frame is considered, it becomes necessary to use the permutation-inversion (PI) group G_{12} shown in Table 1, where the atom labels in Fig. 1 are used to indicate the permutation cycles. In addition, we use in Table 1 the shorthand notation (ab) to represent the full set of eight permuted atoms in the phenyl frame: $(ab)(cd)(45)(67)$.

To set up symmetrized basis set functions and to determine symmetry-allowed terms in the Hamiltonian operator, it is necessary to apply these PI group operations to functions of the torsional angle α and/or the three rotational angles χ, θ, ϕ . For this purpose, we consider the usual [16] equation connecting laboratory-fixed Cartesian coordinates \mathbf{R}_i for each atom to the center of mass \mathbf{R} , to the direction cosine matrix $S^{-1}(\chi, \theta, \phi)$ relating the laboratory-fixed X, Y, Z axes to the molecule-fixed x, y, z axes, and to a second direction cosine matrix $S_i^{-1}(\alpha, 0, 0)$ describing rotation of the methyl group,

$$\mathbf{R}_i = \mathbf{R} + S^{-1}(\chi, \theta, \phi) \left[S_i^{-1}(\alpha, 0, 0) \mathbf{a}_i^0 - \mathbf{A}(\alpha) \right]. \quad (1)$$

We define $S_i^{-1}(\alpha, 0, 0)$ to be the identity matrix for $i \neq 1, 2$, or 3, so that a change in the internal rotation angle α does not affect the

Table 1

Character table for the permutation-inversion group^a G_{12} appropriate for toluene when internal rotation of the methyl group is feasible (see Fig. 1).

	E	(ab)(123)	(123)	(ab) ^b	(23) [*]	(ab)(23) [*]	stat. wt. ^c
	1 ^d	2 ^d	2 ^d	1 ^d	3 ^d	3 ^d	
A_1	1	1	1	1	1	1	5
A_2	1	1	1	1	−1	−1	5
B_1	1	−1	1	−1	1	−1	3
B_2	1	−1	1	−1	−1	1	3
E_1	2	1	−1	−2	0	0	3
E_2	2	−1	−1	2	0	0	5
E	C_{2z}		E	C_{2z}	C_{2y}	C_{2x}	Equivalent rotation ^e

^a This PI group is isomorphic to the point groups C_{6v} , D_{3d} , and D_6 . Here we use a notation that emphasizes the isomorphism with C_{6v} .

^b (ab) in this table is a shorthand notation for the set of four permutations $(ab)(cd)(45)(67)$ in Fig. 1.

^c This column gives the nuclear statistical weights for torsion–rotation levels of the species indicated, for isotopically normal toluene, i.e., for $^{12}\text{C}_7\text{H}_8$.

^d These integers indicate the number of elements in each class. The classes of order 2 contain the element shown and its inverse. The classes of order 3 contain the element shown and two others obtained by replacing (23) by (12) and (13).

^e As defined in [15]. See also Table 2 here.

phenyl frame atoms. For the present paper, we ignore small-amplitude displacement vectors, and consider the \mathbf{a}_i^0 to be constant vectors in an initial coordinate system that puts C_f at the origin, the C_f – C_g bond along the z axis, and all atoms except H_2 and H_3 in the xz plane, as shown in Fig. 1. We also consider the methyl group to have C_{3v} symmetry for the purposes of defining coordinates, so that

$$\mathbf{a}_i^0 = S^{-1}[(2\pi/3)(i-1), 0, 0] \mathbf{a}_1^0 \quad (2)$$

for $i = 1, 2, 3$. The position of the center of mass \mathbf{A} , defined by

$$\mathbf{A}(\alpha, 0, 0) = (1/M) \sum_i m_i S_i^{-1}(\alpha, 0, 0) \mathbf{a}_i^0, \quad (3)$$

is in principle a function of α , but for the symmetrical structure chosen to define our coordinates, \mathbf{A} is in fact a constant vector lying along the z axis.

Table 2 gives the transformations of torsional and rotational coordinates corresponding to the generating operators $(ab)(123)$ and $(23)^*$ for the group in Table 1, as well as for the alternate set of generators (ab) , (123) , and $(23)^*$. The equations above can be used [16] to show that substitution of these transformations on the right side of Eq. (1) does indeed lead to the desired PI operation on the left.

2.2. Allowed terms in the torsion–rotation Hamiltonian

A general expression for the Hamiltonian we use may be written as follows:

$$H = (1/2) \sum_{knpqrs} B_{knpqrs0} \left[J_z^{2k} J_x^n J_y^q J_z^r p_z^s \cos(3s\alpha) + \cos(3s\alpha) p_z^s J_x^n J_y^q J_z^r \right] \\ + (1/2) \sum_{knpqrt} B_{knpqrt} \left[J_z^{2k} J_x^n J_y^q J_z^r p_z^s \sin(3t\alpha) + \sin(3t\alpha) p_z^s J_x^n J_y^q J_z^r \right], \quad (4)$$

where the $B_{knpqrst}$ are fitting parameters; p_z is the angular momentum conjugate to the internal rotation angle α ; J_x, J_y, J_z are projections on the x, y, z axes of the total angular momentum \mathbf{J} . Allowed terms in the torsion–rotation Hamiltonian must be of species A_1 in the group G_{12} of Table 1, must be Hermitian, and must be invariant to the time reversal operation (which for a molecule with an even number of electrons is equivalent to the complex conjugation operation). Since all individual operators $p_z, J_x, J_y, J_z, J^2, \cos 3s\alpha$ and $\sin 3t\alpha$ used in Eq. (4) are Hermitian, all possible terms provided by Eq. (4) will automatically be Hermitian. Therefore, we need only check the terms for symmetry species and time reversal requirements. Table 3 gives the G_{12} symmetry species for the basic operators in Eq. (4), as well as their symmetry under time reversal. By using this table, we find, for example, that both $(J_z J_y + J_y J_z) \sin 3\alpha$ and $(J_z J_x + J_x J_z) \cos 3\alpha$ are Hermitian, invariant under time reversal, and of species A_1 , so each represents a possible term in the Hamiltonian. On the other hand, $J_z \sin 6\alpha$ and $(J_x J_y + J_y J_x)$ each fail one of these criteria, and so cannot occur in the torsion–rotation Hamiltonian.

Table 2
Transformation properties^a of the torsion and rotation^b variables under various operations of the PI group in Table 1.

	α	χ, θ, ϕ
E	α	χ, θ, ϕ
(ab)	$\alpha - \pi$	$\chi + \pi, \theta, \phi$
(123)	$\alpha + 2\pi/3$	χ, θ, ϕ
(ab)(123)	$\alpha - 2\pi/6$	$\chi + \pi, \theta, \phi$
(23)*	$-\alpha$	$\pi - \chi, \pi - \theta, \pi + \phi$

^a When the transformations of α, χ, θ , and ϕ from a given row in this table are substituted into the right side of Eq. (1), the PI operation on the left of that row is obtained on the left of Eq. (1). (See [16] for more details.)

^b Transformations of the rotational angles are used to determine the equivalent rotations [15] given in Table 1.

Table 3
Symmetry species Γ in G_{12} and time reversal symmetry (+) or (–) for some torsional and rotational operators.

Γ	Torsional ^a	Momenta ^b	Laboratory ^c
A_1	$\cos 6\alpha$ (+)		J_x, J_y, J_z
A_2	$\sin 6\alpha$ (+)	J_z (–), p_z (–)	μ_x, μ_y, μ_z
B_1	$\cos 3\alpha$ (+)	J_y (–)	
B_2	$\sin 3\alpha$ (+)	J_x (–)	
E_1	$\exp(\pm i\alpha)$		
E_2	$\exp(\pm 2i\alpha)$		

^a The column headed Torsional contains trigonometric functions of the torsional angle.

^b The column headed Momenta contains the torsional angular momentum and the molecule-fixed components of the total angular momentum operator.

^c The column headed Laboratory contains the laboratory-fixed components of the dipole moment operator and of the total angular momentum operator.

2.3. Determination of the sign of V_6

Sørensen and Pedersen were the first to recognize that the sign of V_6 can be determined from microwave spectra [3] when certain torsion–rotation operators allowed in G_{12} but forbidden in the group G_{24} proposed earlier for molecules with a sixfold barrier [1] become important, e.g., $J_y[p_z \sin(3\alpha) + \sin(3\alpha)p_z]$ and $J_x[p_z \cos(3\alpha) + \cos(3\alpha)p_z]$. In their treatment of the CD_3NO_2 spectrum, they considered two potential functions, one of the form $(1/2)V_6(1 - \cos 6\alpha)$, the other of the form $(1/2)V_6(1 + \cos 6\alpha)$. The first of these has a minimum energy of 0 at $\alpha = 2n\pi/6$ for integer n , and a maximum energy of V_6 at $\alpha = (2n+1)\pi/6$ for integer n , whereas the second has a maximum energy of V_6 at $\alpha = 2n\pi/6$ for integer n , and a minimum energy of 0 at $\alpha = (2n+1)\pi/6$ for integer n . Sørensen and Pedersen found [3] that the standard deviation of their fits with the two different sign choices differed by a factor of 5, when 67 lines with $J \leq 10$ were included, and that this difference rose to a factor of 100 when high- J lines were added. The sign in the sixfold potential function can thus be determined from a fit, and structural information about the methyl group orientation can be obtained, which is quite different from the corresponding sign in the threefold potential function appropriate for methanol-like molecules. We now give a slightly more pictorial description of how this happens.

From a physical point of view, the two terms in the preceding paragraph arise because of changes in the perpendicular Coriolis energy contributions caused by various bond-length and bond-angle relaxations that occur during internal rotation of the methyl group. These terms must be added to the Hamiltonian because such structural relaxations along the internal-rotation path are neglected in the highly symmetric definition of the internal-rotation motion implied by Eqs. (1)–(3). The influence of these two Coriolis terms on the rotational energy levels of toluene can be understood qualitatively as follows. If the potential energy function has the form $(1/2)V_6(1 - \cos 6\alpha)$, then the equilibrium conformation occurs at $\alpha = 0$ and the top of the well occurs at $\pi/6$, so that the $J_x[p_z \cos(3\alpha) + \cos(3\alpha)p_z]$ term is nonvanishing at the bottom of the well while the $J_y[p_z \sin(3\alpha) + \sin(3\alpha)p_z]$ term is nonvanishing at the top. This corresponds to a b -axis Coriolis contribution to the energy at the bottom of the well (in the coordinate system of this paper) and a c -axis contribution at the top. If, on the other hand, the potential energy function for toluene has the form $(1/2)V_6(1 + \cos 6\alpha)$, then the equilibrium conformation occurs at $\alpha = \pi/6$ and the top of the barrier occurs at $\alpha = 0$, corresponding to a c -axis Coriolis contribution to the energy at the bottom of the well and a b -axis contribution at the top. These two “gyroscopic” situations are physically different, and can thus be distinguished by examining the standard deviation of fits of torsion–rotation transitions.

Consider next for comparison the case of acetaldehyde CH_3CHO , with $\alpha = 0$ defined as the configuration where H_1 of the methyl group eclipses the O of the aldehyde group. If the potential energy function has the form $(1/2)V_3(1 - \cos 3\alpha)$, then the bottom of the well occurs at $\alpha = 0$ and the top occurs at $\alpha = \pi/3$. If the potential energy function has the form $(1/2)V_3(1 + \cos 3\alpha)$, then the bottom of the well occurs at $\alpha = \pi/3$ and the top at $\alpha = 0$. Thus for either sign choice in the V_3 potential, $J_y[p_x \sin(3\alpha) + \sin(3\alpha)p_x]$ is zero and $J_x[p_x \cos(3\alpha) + \cos(3\alpha)p_x]$ is non-zero at both the bottom and the top of the well, i.e., the two different forms of the potential function allow a b -type Coriolis contribution and forbid a c -type contribution to the energy at both the top and bottom of the well. The “gyroscopic” situations for the two forms of the V_3 potential function can therefore, not be distinguished simply by examining the quality of fits to torsion–rotation transitions.

Further discussion of the determinability of the potential function sign as well as of our fitting results for toluene for both sign choices is presented in Section 6.

2.4. Basis-set functions for the two-step diagonalization procedure

In both diagonalization steps of the present computer program, we do not actually make use of the full PI group G_{12} , but operate implicitly with a subgroup G_6 of this group that does not distinguish between the subscripts 1 and 2 on the A and B species. This group is isomorphic with the point group C_6 , and has the advantage, as explained in the footnotes of Tables 4 and 5, that symmetry species identification and multiplication can be carried out using integer arithmetic modulo 6, i.e., using arithmetic involving “only” the integers 0, ± 1 , ± 2 , and 3.

Table 4 gives the character table for this G_6 group, which can be seen to contain complex characters. Since the introduction of symmetry species with complex characters leads to some changes in the real group-theoretical equations most familiar to molecular spectroscopists, we give in Table 5 the multiplication table for the species of G_6 in Table 4. We also note that Table 4 contains two “separably” degenerate E species [17]. Briefly, a separably degenerate E species is a reducible doubly degenerate representation with real characters that contains two irreducible non-degenerate representations with complex characters. Based on group-theoretical considerations alone, the two irreducible representations with complex characters would be assumed to have different energies at some level of measurement accuracy, but the time reversal symmetry operation (which is essentially the operation of complex conjugation for systems with integral electron spin) requires them to have equal energies. We use the idea of separably degenerate species here only to avoid redundant energy computations.

Table 4

Character table for the subgroup G_6^a of G_{12} needed to understand basis set construction^b in the two-step diagonalization procedure used here.

Γ	$\sigma(\Gamma)$	C_6^0 E	C_6^1 (ab)(123)	C_6^2 (123) ²	C_6^3 (ab)	C_6^4 (123)	C_6^5 (ab)(123) ²	$\exp(6s + \sigma_t)i\alpha$ σ_t	$ KJM\rangle$ K
A	0	ϵ^0	ϵ^0	ϵ^0	ϵ^0	ϵ^0	ϵ^0	0	Even
E_{1+}	+1	ϵ^0	ϵ^{+1}	ϵ^{+2}	ϵ^{+3}	ϵ^{+4}	ϵ^{+5}	+1	
E_{1-}	-1	ϵ^0	ϵ^{-1}	ϵ^{-2}	ϵ^{-3}	ϵ^{-4}	ϵ^{-5}	-1	
E_{2+}	+2	ϵ^0	ϵ^{+2}	ϵ^{+4}	ϵ^0	ϵ^{+2}	ϵ^{+4}	+2	
E_{2-}	-2	ϵ^0	ϵ^{-2}	ϵ^{-4}	ϵ^0	ϵ^{-2}	ϵ^{-4}	-2	
B	3	ϵ^0	ϵ^3	ϵ^0	ϵ^3	ϵ^0	ϵ^3	3	Odd

^a This PI group is isomorphic to the point group C_6 , with the PI elements along the top of the table corresponding to C_6^p , with $p = 0, 1, 2, 3, 4$, and 5. Every element is in its own class. All irreducible representations are therefore non-degenerate, and some have complex characters. The irreducible representations with complex characters can be combined in pairs to give reducible representations with only real characters (e.g., $E_1 = E_{1+} \oplus E_{1-}$ or $E_2 = E_{2+} \oplus E_{2-}$). These are called separably degenerate E species. To illustrate the simple structure of the character table, all characters are expressed as powers of $\epsilon \equiv \exp(-2\pi i/6)$. The exponents n of ϵ^n in the column headed by (ab)(123) define an integer $\sigma(\Gamma) = n \text{ modulo } 6$ associated with each irreducible representation Γ of this PI group.

^b The last two columns indicate the symmetry species of torsional functions of the form $\exp(6s + \sigma_t)i\alpha$, where s and σ_t are integers, and of the symmetric-rotor functions with even and odd K . Note that the σ_t values in the $\exp(6s + \sigma_t)i\alpha$ column agree with the $\sigma(\Gamma)$ values in the same row.

Table 5

Multiplication^a table for species of the subgroup G_6 of G_{12} needed to understand basis set construction in the two-step diagonalization procedure used here.

Γ	A	B	E_{1+}	E_{1-}	E_{2+}	E_{2-}
A	A	B	E_{1+}	E_{1-}	E_{2+}	E_{2-}
B	B	A	E_{2-}	E_{2+}	E_{1-}	E_{1+}
E_{1+}	E_{1+}	E_{2-}	E_{2+}	A	B	E_{1-}
E_{1-}	E_{1-}	E_{2+}	A	E_{2-}	E_{1+}	B
E_{2+}	E_{2+}	E_{1-}	B	E_{1+}	E_{2-}	A
E_{2-}	E_{2-}	E_{1+}	E_{1-}	B	A	E_{2+}

^a This multiplication table can be constructed simply by adding σ values of the two symmetry species in a product to obtain the final σ value, i.e., $\sigma(\Gamma_1 \times \Gamma_2) = \sigma(\Gamma_1) + \sigma(\Gamma_2)$, where $\sigma(\Gamma)$ is defined in Table 4.

In the first diagonalization step we consider separately blocks in the Hamiltonian matrix characterized by a given value of σ_t and K in the basis set $[\exp(6s + \sigma_t)i\alpha] |KJM\rangle$, where s is a positive or negative integer, so that the torsion–rotation (tr) symmetry species ${}^tr\Gamma$ in G_6 of all basis functions in any block is given by

$${}^tr\Gamma = {}^t\Gamma(\sigma_t) \times {}^r\Gamma(K) \quad (5a)$$

$$\sigma_{tr} = \sigma_t + \sigma_r \text{ modulo } 6, \quad (5b)$$

where σ_t is taken from the torsional basis function and $\sigma_r = 0$ or 3 for even or odd values of K , respectively (see Table 4).

In the second diagonalization step we must consider together all functions of different K having the same torsion–rotation symmetry ${}^tr\Gamma$ (i.e., having the same σ_{tr}). Tables 4 and 5 indicate, for example, that basis set functions $[\exp(6s + \sigma_t)i\alpha] |KJM\rangle$ having $\sigma_t = 0$ and $K = \text{even}$ must be put in the same ${}^tr\Gamma = A$ matrix ($\sigma_{tr} = 0$) as functions having $\sigma_t = 3$ and $K = \text{odd}$, or that torsion–rotation basis functions having $\sigma_t = +1$ and $K = \text{even}$ must be put in the same $\Gamma = {}^{tr}E_{1+}$ matrix ($\sigma_{tr} = +1$) as functions having $\sigma_t = -2$ and $K = \text{odd}$, etc. Because separably degenerate species correspond to degenerate energy levels for a Hamiltonian without external fields, it is only necessary to diagonalize blocks with ${}^tr\Gamma = A, E_{1+}, E_{2+}$, and B in the second step, corresponding, respectively, to our choice of $\sigma_{tr} = 0, 1, 2$, and 3 in the program.

2.5. Torsional and rotational labels for eigenvectors after the first diagonalization

For the internal-rotation Hamiltonian with a sixfold barrier,

$$H = Fp_x^2 + (1/2)V_6(1 \pm \cos 6\alpha), \quad (6)$$

we can consider two limiting cases for the torsional labels, just as for the threefold barrier problem. In the high barrier limit, all levels of interest are well below the top of the barrier V_6 , and their ener-

gies are essentially those of a harmonic oscillator, given by $(v_t + 1/2)h\nu$, with $\nu = (36FV_6)^{1/2}$ (when F and V_6 are in their appropriate SI units). In the low-barrier limit, all levels of interest are well above the top of the barrier, and their energies are essentially those of a particle on a ring, given by Fm^2 . Molecules with a sixfold barrier and a CH_3 top are normally close to the low-barrier limit, so we have used m as a torsional label at all stages of our fitting program. (Note, however, that replacing the CH_3 top in any given molecule by a much heavier CF_3 top, could result in a change from low-barrier to intermediate or high barrier.)

The m labeling scheme after the first diagonalization step is based on energy ordering, rather than on eigenfunction composition. The exact scheme is as follows. For the lowest eigenvalue in a matrix characterized by $\sigma_t = 0, 1, 2$, or 3 , we choose $m = \sigma_t$. For the next four eigenvalues in ascending energy order, we choose $m = \sigma_t - 6, \sigma_t + 6, \sigma_t - 12, \sigma_t + 12$. Extension of the m labels to higher eigenvalues follows the same pattern. While the m labeling scheme described above provides a unique and easily programmed set of labels, the m label for a given level does not always correspond to the $m = 6s + \sigma_t$ value of the torsional basis function with the largest coefficient in the eigenfunction for that level. This is especially true for states with $m = \pm 3, \pm 6$, etc., i.e., for $0 \neq m = 3$ or $6 \pmod 6$.

K labels for eigenfunctions after the first diagonalization are automatic, since each matrix in the first step is characterized by a fixed value of K .

2.6. Torsional and rotational labels for eigenvectors after the second diagonalization

The labeling scheme after the second diagonalization begins by using eigenfunction composition to determine the m state (as described above) to which a particular level belongs, and then uses the usual asymmetric-rotor energy ordering scheme to assign rotational K_a, K_c labels within a given m state. Our asymmetric-rotor K_a, K_c labels are thus based on energy ordering. They are unique and easily programmed, but they frequently do not correspond to the K value of the rotational basis function with the largest coefficient in the eigenvector when such a dominant component exists. Some additional aspects of the torsion-rotation labels described above are discussed in Section 5.

Because our K labels after the second diagonalization are based on energy ordering, rather than on eigenvector composition, intensities for transitions between all eigenvectors in each pair of J' and J'' manifolds are calculated in the program (see Section 3), to prevent overlooking strong transitions involving unexpected changes in m or K .

2.7. Recovery of the 1 and 2 subscripts on the A and B functions after the second diagonalization

It is sometimes desirable to put the 1 or 2 subscript on a given eigenfunction from the ${}^t\Gamma = A$ or B symmetry block, i.e., it is sometimes desirable to work with symmetry species of the full G_{12} PI group. This can be done by taking the expectation value of the symmetry operation $(23)^*$, since an expectation value of $+1$ indicates A_1 or B_1 , while a value of -1 indicates A_2 or B_2 . Of course, if an A_1/A_2 pair or a B_1/B_2 pair is degenerate to within machine round-off error, then the eigenvectors returned by the diagonalization algorithm will be random linear combinations of the subscript 1 and 2 states, leading to expectation values of $+p$ and $-p$, respectively, where $-1 \leq p \leq +1$. The magnitude of p will approach unity only if the splitting is orders of magnitude larger than machine round-off error. These incompletely resolved degeneracies will arise frequently and systematically for high- K_a states with small asymmetry doublings.

Table 2 indicates that for our first-stage basis set of $[\exp(6s + \sigma_t)ix] |KJM\rangle$, the matrix elements of $(23)^*$ are given by Eqs. (7a) and (7b), respectively, for basis functions with tA ($\sigma_t = 0$) and tB ($\sigma_t = 3$) torsional symmetry:

$$\langle {}^tA; s'K'J | (23)^* | {}^tA; sKJ \rangle = \delta(s', -s)\delta(K', -K)(-1)^{J-K} \quad (7a)$$

$$\langle {}^tB; s'K'J | (23)^* | {}^tB; sKJ \rangle = \delta(s', -s-1)\delta(K', -K)(-1)^{J-K}. \quad (7b)$$

Applying Eqs. (7a) and (7b) to the second-stage eigenfunctions, we calculate in our program the expectation value for $(23)^*$ for $\sigma_{tr} = 0$ and 3 and thus determine A_1/A_2 and B_1/B_2 labels for non-degenerate states.

3. Structure of the computer program

The computer program uses the two step diagonalization procedure of Herbst et al. [18], similar to that implemented in BELGI [19,20]. In the first step a set of torsional calculations is performed with a relatively large torsional basis set of the form $\exp[(6s + \sigma_t)ix]$ for each value of K in the range $-J_{max} \leq K \leq +J_{max}$, and for each of the four different values of $isig \equiv \sigma_t$ ($isig = 0, +1, +2, +3$). In this step only Hamiltonian matrix elements diagonal in K are considered, and usually only the main purely torsional effects together with the torsion-rotation coupling about the inertial a axis are taken into account. In the second step a reduced torsional basis set is used, which is obtained by discarding all but the lowest several torsional eigenfunctions for a given K and $isig$ from the first step. Although the size of the basis set in the first step can be varied by choosing a value for $ktronc$ (where $|s| \leq ktronc$), and the number of torsional eigenfunctions kept in the second step may be varied by choosing a value for nvt , we currently use 21 basis functions in the first step and 9 in the second, as it is often done in fits using BELGI [21]. In the second step, a separate matrix of dimension $(2J+1)*nvt \times (2J+1)*nvt$ is built for each pair of ($isig \equiv \sigma_{tr}, J$) values, and all desired asymmetric-rotor and torsion-rotation K mixing effects are taken into account.

In the Hamiltonian matrix of the second diagonalization step we group together basis set functions of given K value, in contrast to BELGI, where the basis set functions are grouped by torsional quantum number. Because interaction terms are normally limited to some maximum value of $|\Delta K|$, this leads to a banded structure for the matrix, which becomes more pronounced as J increases, and which permits the use of efficient diagonalization routines that take advantage of this special matrix structure. We use the DSRDRT routine from the Successive Band Reduction (SBR) package [22] to reduce the banded matrix to tridiagonal form and then use the corresponding LAPACK [23] routines to get eigenvalues and eigenvectors of the obtained tridiagonal matrix.

In the program, matrix elements for specific terms in the general expression of Eq. (4) are calculated, which the user selects via sets of k, n, p, q, r, s, t integer indices in the input file. During input, each set of k, n, p, q, r, s, t integer indices is checked for conformity with time reversal and symmetry requirements, to prevent accidental introduction of symmetry-forbidden terms into the Hamiltonian. It is also possible at input to define a linear combination of several different terms as a sum with fixed coefficients, with that sum then being multiplied by one fitting parameter. A conventional weighted least squares fit is carried out, with special treatment for blended transitions, where an intensity-weighted average of calculated (but experimentally unresolved) transition frequencies is put in correspondence with the measured blended-line frequency.

Intensity calculations for rotation-torsion transitions are similar to those in BELGI [20,21]. Such intensity calculations are particularly important for the low-barrier case of toluene, because normal asymmetric-rotor selection rules are not always a good

guide for deciding the strongest lines. For this reason, the program calculates all possible ΔK_a , ΔK_c transition frequencies and intensities allowed by symmetry in G_{12} for a given pair of upper and lower state J values, and displays all transitions with intensities above a user-set cutoff.

A convenient check of the program code for many of the higher-order terms was obtained by verifying that eigenvalues E and W of the Hamiltonians H and $H(1+\beta H)$, respectively, satisfy $W = E(1 + \beta E)$ to machine round-off error. For example, if

$$H = F(P_x - \rho J_z)^2 + (1/2)V_6(1 - \cos 6\alpha) \quad (8)$$

has eigenvalues E_i , and if

$$\begin{aligned} H + \beta H^2 = & F(P_x - \rho J_z)^2 + (1/2)V_6(1 - \cos 6\alpha) \\ & + \beta F^2(P_x^4 - 4P_x^3\rho J_z + 6P_x^2\rho^2 J_z^2 - 4P_x\rho^3 J_z^3 + \rho^4 J_z^4) \\ & + \beta F V_6(P_x - \rho J_z)^2 - (1/2)\beta F V_6\{(P_x - \rho J_z)^2, \cos 6\alpha\} \\ & + (1/8)\beta V_6^2(3 - 4\cos 6\alpha + \cos 12\alpha), \end{aligned} \quad (9)$$

where $\{A, B\} \equiv AB + BA$, has eigenvalues $E_i + \beta E_i^2$, then there is a high probability that all terms in these two expressions are correctly programmed. Because of the peculiarities of our two-step diagonalization algorithm, where some operators are included in the first step, with a larger torsional basis set, while others are introduced only in the second step, with a truncated torsional basis set (as described above), the numerical check to machine round-off precision described in this paragraph is possible only if the torsional basis set is not truncated in the second step. Furthermore, agreement to machine round-off error could not be achieved for a (variable) range of the highest-energy eigenvalues because eigenvalues of the square of an operator with off-diagonal matrix elements are not exactly equal to the square of eigenvalues of that operator, when those eigenvalues are determined by diagonalizing matrices set up in a truncated basis set.

It is our intention, after this program has been tested by application to a few more example molecules, to make it available for general use on the PROSPE website [20].

4. Experimental

The ground state ($m = 0$) data used in this work are a subset of the measurements published in [11], in that only transitions with $J \leq 30$ and $K_a \leq 12$ were used. The higher m measurements were made with three of the spectrometers used in [11]. The majority of the measurements were carried out at room-temperature with two different Fourier transform (FT) waveguide instruments in Kiel. Transitions in the 8–18 GHz region were measured with a spectrometer using a rectangular absorption cell and capable of automatic scanning [24,25]. The scanning feature was crucial in commencing the assignment since it allowed recording of broad regions of the spectrum centered on successive relevant multiples of $(B + C)$. Those regions were expected to contain the free-rotation bandheads formed by low- J R -branches and were the key to initial assignment of the higher m states. Transitions in the 18–26.5 GHz region were measured with a Fourier transform waveguide spectrometer employing a 36 m long circular waveguide cell [26]. This region was used to confirm the assignment of lower- J R -branch transitions and both regions were used in searches for Q -branch transitions.

The third spectrometer was the pulsed supersonic expansion Fourier transform cavity spectrometer in Warsaw [27], operating at 2–18.5 GHz. Although the efficiency of cooling obtained on supersonic expansion is so high that it normally prohibits observation of vibrationally excited transitions in this spectrometer, there is a special case when those transitions involve a lower state of

symmetry having different nuclear spin statistics from those of the ground state. This phenomenon of cooling of populations to the lowest A -symmetry and lowest E -symmetry states allowed observation of strong $m = 1$ transitions in the supersonic expansion.

For weighting purposes in the least squares fits, where we take weight = $(1/\text{uncertainty})^2$, transitions in the data set were assigned a frequency uncertainty of 2 kHz for the supersonic expansion measurements and 5 kHz for the waveguide FT measurements. For weaker transitions, uncertainties were increased to 4 kHz for supersonic expansion and 10, 20 or 50 kHz for waveguide data.

5. Qualitative understanding of the energy levels

The low-barrier torsion–rotation energy levels of toluene for various m states can be understood qualitatively by examining levels obtained from an approximate Hamiltonian containing only the lowest-order torsional and rotational terms and having the z axis along the principal a axis,

$$H = F(P_x - \rho J_z)^2 + (1/2)V_6(1 + \cos 6\alpha) + A J_z^2 + B J_x^2 + C J_y^2, \quad (10)$$

together with the concept of an approximate effective rotational Hamiltonian $H_m(\text{rot})$. For each m , we obtain the effective rotational Hamiltonian by taking the expectation value of Eq. (10) in a free-rotor basis set to obtain [28]

$$\begin{aligned} H_m(\text{rot}) = & \langle m | H | m \rangle \\ = & (1/2)V_6 + Fm^2 - 2F\rho m J_z + B J_x^2 + C J_y^2 \\ & + (A + \rho^2 F) J_z^2. \end{aligned} \quad (11)$$

We will compare the approximate energy levels from Eq. (11) with those calculated from constants obtained from our global fit and plotted against $J(J + 1)$. The four panels of Fig. 2 show such calculated toluene levels for $|m| = 0, 1, 2$, and 3, though the levels displayed are actually reduced levels of the form $E(m, J, K) - 0.5(B + C)J(J + 1)$, so that a large part of the J -dependence has been removed.

For $m = 0$, Eq. (11) becomes

$$\begin{aligned} H_0(\text{rot}) = & \langle m = 0 | H | m = 0 \rangle \\ = & (1/2)V_6 + B J_x^2 + C J_y^2 + (A + \rho^2 F) J_z^2 \end{aligned} \quad (12)$$

which, as is well known [28], has the form of an asymmetric-rotor Hamiltonian with $A_{\text{eff}} = A + \rho^2 F$. For toluene, the A_{eff} modification is slight. Our fitting results give a value of $A_{\text{eff}} = 0.1911 \text{ cm}^{-1}$ (which is in complete agreement with the asymmetric-rotor fit carried out for $m' = m'' = 0$ transitions in [11]), as well as $\rho^2 F = 0.0066 \text{ cm}^{-1}$ and $A = 0.1845 \text{ cm}^{-1}$.

For low- J levels, where the term $(1/2)(B - C)(J_x^2 - J_y^2)$ representing asymmetric-rotor effects can be neglected, the eigenvalues E of Eq. (12) give rise to reduced energy levels of the form

$$E(J, K) - (1/2)(B + C)J(J + 1) = (1/2)V_6 + [A_{\text{eff}} - (B + C)/2]K^2, \quad (13)$$

where K is the angular momentum projection along the principal a axis. As the eigenvalue of J_z in Eqs. (10) and (11), K is taken in this section to be a signed quantity. Fig. 2(a) does indeed show, as expected from Eq. (13), a series of nearly straight, nearly horizontal lines, with the line beginning on the left with a point at $J = K$ having an approximate reduced energy of $(1/2)V_6 + [A_{\text{eff}} - (B + C)/2]K^2$. Deviations from horizontal straight line behavior at low K are due to asymmetric-rotor effects. Asymmetry splittings can be seen for $K = 7$ and below on the scale of this figure.

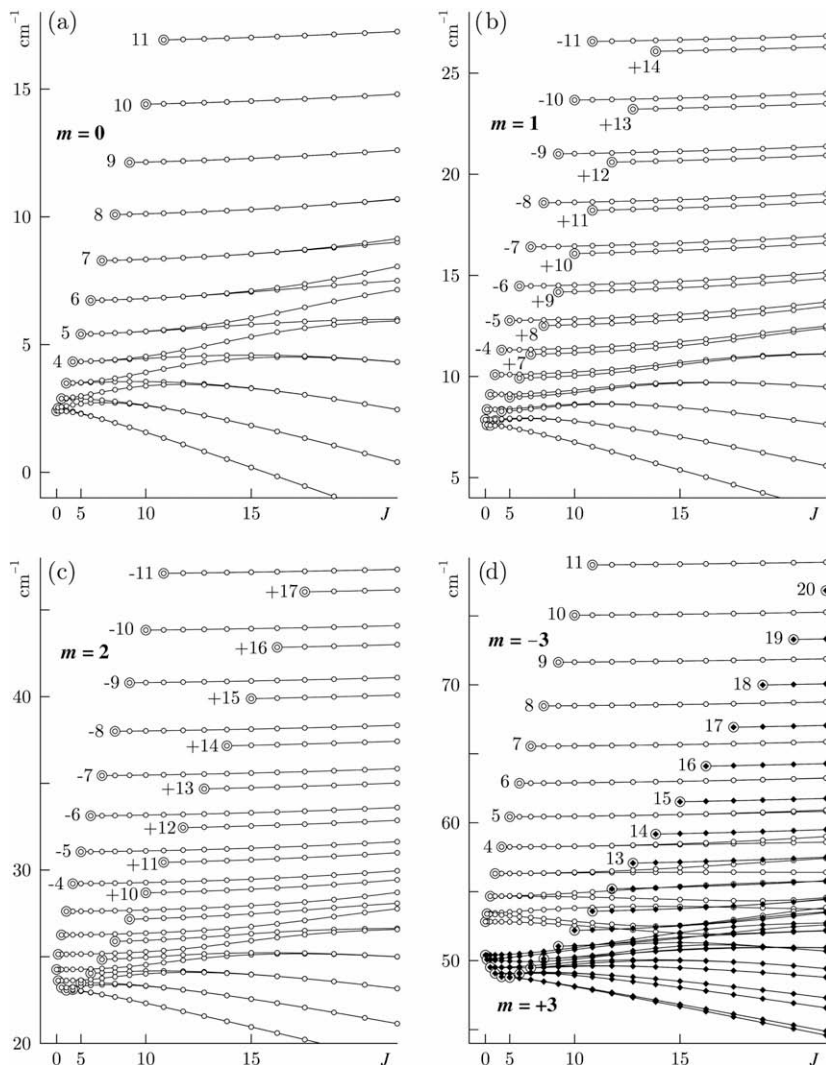


Fig. 2. Reduced energy levels $E - (1/2)(B + C)J(J + 1)$ for torsional states of toluene with $m = 0, 1, 2$, and ± 3 plotted against $J(J + 1)$ (though the abscissa is labeled in J), as calculated from our program. Most of the reduced energy levels can be organized into nearly straight, nearly horizontal lines. The lowest- J level of each horizontal line is circled, and K labels are given near the circled points where space permits. These K labels are determined by setting $K = J$ for the circled points. Panel (a) shows that the circled levels for $m = 0$ increase in energy as K^2 . Panels (b) and (c) show that these levels for $m = 1$ and 2 fall on curves resembling a parabola tilted to the right. Panel (d) shows that the circled levels for $|m| = 3$ fall on a similar tilted parabolic curve, except that a gap of $(1/2)V_6 \approx 2.5 \text{ cm}^{-1}$ has been opened at $J = 0$ by the sixfold barrier term (see text). Levels on the part of the tilted parabola starting below the gap in panel (d) are called $m = +3$ levels in the program. Levels starting above the gap are called $m = -3$. Torsion-rotation energy levels with $m = 0, +3$, and -3 belong to non-degenerate A symmetry species in G_{12} , and their K values are unsigned, indicating that a pair of $\pm K A$ levels have the same energy on the scale of this figure. Torsion-rotation energy levels with $m = 1$ and 2 belong to doubly degenerate E species. K values on the left limb of the inclined parabolas in panels (b) and (c) are all negative (for positive m), while those on the right limb are all positive. Note also how the parabolas gradually become wider on going from $m = 0$ to $|m| = 3$.

For the $|m| = 1$ states, Eq. (11) becomes

$$H_{\pm 1}(\text{rot}) = \langle m = \pm 1 | H | m = \pm 1 \rangle \\ = (1/2)V_6 + F \mp 2\rho F J_z + (A + \rho^2 F)J_z^2 + B J_x^2 + C J_y^2. \quad (14)$$

Interactions between $m = +1$ and -1 states vanish, since

$$\langle m = \mp 1 | H | m = \pm 1 \rangle = 0, \quad (15)$$

which is just an expression of the fact that matrix elements of $\cos 6\alpha$ within the two $|m| = 1$ torsional states vanish. Thus, for the $|m| = 1$ states, we need consider only $m = +1$ by itself, since: (i) the upper and lower signs in Eq. (14) give rise to the same expressions when K takes all values $-J \leq K \leq +J$, and (ii) $m = +1$ and -1 do not interact. However, the presence of the term linear in J_z in Eq. (14) means that eigenvalues of Eq. (14) will not resemble those of an asymmetric rotor.

For low- J levels, where asymmetric-rotor effects can be neglected, the eigenvalues E of Eq. (14) for $m = +1$ give rise to reduced energy levels of the form

$$E(J, K) - (1/2)(B + C)J(J + 1) = (1/2)V_6 + F - 2\rho F K + [A_{\text{eff}} \\ - (B + C)/2]K^2, \quad (16)$$

where K is again taken to be a signed quantity. This expression can be compared with the low- J $m = +1$ reduced energy levels calculated from our fitting constants and shown in Fig. 2(b). As predicted by Eq. (16), most reduced energy levels in this figure organize themselves into nearly straight, nearly horizontal lines, whose $|K|$ value can be determined from the lowest J value (left-most point on the line). Furthermore, the curve connecting the first point of each straight line, i.e., the curve connecting the circled $J = |K|$ levels in Fig. 2(b), has the form of an inclined (and distorted) parabola, whose lowest point is predicted (by differentiating Eq. (16) with respect to K) to occur at $K \approx +\rho F/[A_{\text{eff}} - (B + C)/2] = 1.6$. This prediction is in reasonable agreement with Fig. 2(b), where the two lowest lines for $m = +1$ have $K = +1$ and $K = +2$. More information on parabolas can be found in related discussions [29,30] of nearly free-rotor

torsion–rotation energy levels plotted against K . Note finally that the splitting patterns of these $J = |K|$ levels cannot be forced into an asymmetric-rotor-like pattern, since normal asymmetry splittings (as in Fig. 2(a)) nearly vanish when $J = |K|$, whereas no pairs of nearly degenerate $J = |K|$ levels with the same $|K|$ can be found in Fig. 2(b).

Using arguments similar to those for $|m| = 1$, the reduced energy level expression for $|m| = 2$ is found to be

$$E(J, K) - (1/2)(B + C)J(J + 1) = (1/2)V_6 + 4F - 4\rho FK + [A_{\text{eff}} - (B + C)/2]K^2 \quad (17)$$

This expression can be compared with Fig. 2(c), which gives the $|m| = 2$ reduced energy levels obtained from our fit. Eq. (17) predicts that the reduced energy levels in Fig. 2(c) will organize themselves into straight horizontal lines, with the lowest-energy point of the inclined parabola connecting the circled $J = |K|$ levels occurring at $K \approx +2\rho F/[A_{\text{eff}} - (B + C)/2] = 3.2$. This predicted behavior is again in reasonable agreement with the observed behavior in Fig. 2(c), where the two lowest lines for $m = +2$ have $K = +3$ and $K = +4$. The $|m| = 2$ splitting patterns can also not be forced into an asymmetric-rotor-like pattern.

For $|m| = 3$ the calculation of the effective rotational Hamiltonian is somewhat different [28], because $V_6 \cos 6\alpha$ has nonvanishing matrix elements within the $|m| = 3$ torsional states (i.e., between $m = +3$ and $m = -3$), leading (when this term dominates other interactions) to sum and difference torsional eigenfunctions. Without this interaction we obtain from Eq. (11) the effective rotational Hamiltonian

$$H_{\pm 3}(\text{rot}) = \langle m = \pm 3 | H | m = \pm 3 \rangle = (1/2)V_6 + 9F \mp 6\rho F J_z + (A + \rho^2 F)J_z^2 + B J_x^2 + C J_y^2. \quad (18)$$

Introduction of the $(1/2)V_6 \cos 6\alpha$ interaction between the close-lying $m = \pm 3$ components, gives the off-diagonal matrix elements

$$H_3(\text{rot}) = \langle m = \pm 3 | H | m = \mp 3 \rangle = (1/4)V_6, \quad (19)$$

and leads to a 2×2 diagonalization, giving the pair of effective rotational Hamiltonians

$$H_{3\pm}(\text{rot}) = (1/2)V_6 + 9F + (A + \rho^2 F)J_z^2 + B J_x^2 + C J_y^2 \pm [(1/16)V_6^2 + 36F^2 \rho^2 J_z^2]^{1/2}. \quad (20)$$

The square root in Eq. (20) will obviously give rise to rather complicated energy level patterns for $|m| = 3$ levels. Some simplification of Eq. (20) can be achieved when either the V_6 term or the $F\rho J_z$ dominates, since then the square root can be expanded in a Taylor series, but these cases will not be considered here since neither term dominates for toluene.

Eq. (18) would predict a diagram very similar to Fig. 2(b) and (c), with the lowest point on the parabola occurring for $K \approx 4.7$. The effect of the off-diagonal $(1/2)V_6 \cos 6\alpha$ interaction in Eq. (19) is to open up a gap of $(1/2)V_6$ between the $K = 0$ levels with $m = +3$ and $m = -3$ and to slightly modify the shape of the inclined parabola. This is in good qualitative agreement with our calculated $|m| = 3$ levels, as shown in Fig. 2(d).

Up to this point we have been considering torsion–rotation levels in Fig. 2 only for low J . As is well known, at very high J and very low K_a , the rotational levels of a prolate asymmetric-rotor regroup themselves into K_c clusters [31]. The same phenomenon occurs here, as illustrated by the torsion–rotation levels at the bottom right in each of the four panels of Fig. 2, but the K_c spacings are slightly modified by torsion–rotation interaction. The spacing can be understood by considering a Hamiltonian with the z axis along the principal c axis, i.e., by performing $(x, y, z) \rightarrow (y, z, x)$ on Eq. (10) to obtain

$$H = F(P_x - \rho J_x)^2 + (1/2)V_6(1 + \cos 6\alpha) + A J_x^2 + B J_y^2 + C J_z^2 = (1/2)V_6 + F P_x^2 + (1/2)(A_{\text{eff}} + B)J^2 + [C - (1/2)(A_{\text{eff}} + B)]J_z^2 - 2F\rho P_x J_x + (1/2)(A_{\text{eff}} - B)(J_x^2 - J_y^2) + (1/2)V_6 \cos 6\alpha. \quad (21)$$

(Since K is now the projection of \mathbf{J} along the principal c axis, we call it K_c in this paragraph to avoid confusion.) A second-order perturbation calculation (with the last three terms in Eq. (21) as the perturbation), gives a value of 2.24 cm^{-1} for the spacing between the $K_c = 19$ and 20 toluene levels with $m = 2$ and $J = 20$. This value differs by only 2% from the value of 2.20 cm^{-1} calculated by the program. This good agreement demonstrates that the K_a, K_c labels used in the program have their usual connection to asymmetric-rotor energy level patterns and selection rules for levels with high J and high K_c . The various panels in Fig. 2 indicate, however, that the K_a, K_c labels used in the program do not have their usual asymmetric-rotor meaning for levels with low J and low K_a . Since there is no K_a, K_c labeling scheme which will provide straightforward physical meaning for the whole range of rotational quantum numbers, we use in the program (and in the tables of line frequencies below) the unique and simply automated labeling scheme described earlier, while recognizing that these K_a, K_c labels from the program must be changed in an appropriate way when trying to extract qualitative understanding of the energy level pattern for some ranges of rotational quantum numbers.

6. Discussion of the molecular constants determined in the fit

Table 6 presents the $m = 1, 2, \pm 3$ and $m = +3 \leftrightarrow m = -3$ transition frequencies of toluene used in the least squares fit, together with their assignments, measurement uncertainties and observed-minus-calculated (o–c) residuals. The $m = 0$ lines can be found in [11]. (All lines included in the fit and their residuals are given in the computer output in the archived material.) Transitions in Table 6 are grouped into spectroscopic branches. The random distribution of residuals along these branches suggests that any quantum number-related model inadequacies are below measurement accuracy. An overview of the results in Table 6 is given in Table 7, where measurements are divided on the left according to upper and lower torsional state, and on the right according to assigned measurement precision. It can be seen that we have satisfactory observed-minus-calculated residuals for each category of lines, although there is somewhat better J quantum number coverage and more measured lines for $m = 0$ and $+3$ states, than for $m = 1$ and 2 states. This slight disproportion is a consequence of: (i) frequency range limitations, (ii) the previous very thorough study of the $m = 0$ spectrum, and (iii) the energy level structure of the $m = +3$ state (see Fig. 2d), which puts many Q -type transitions within the frequency range of our current study.

Table 8 gives the set of molecular constants determined in the fit, both in the B_{knprst} notation of Eq. (4) and in a more descriptive notation [32]. Although a great deal is known about the low-order constants of toluene from previous work, some additional remarks are of interest. It can be seen that our set of 28 constants consists of 2 pure torsional constants, 8 pure rotational constants, and 18 torsion–rotation interaction constants. In terms of the ordering scheme introduced by Nakagawa et al. [33], which is extensively used for torsion–rotation Hamiltonians with threefold barriers (see for example [21,32]), we have used terms up to 8th order, with the number of terms distributed between the $n = 2, 4, 6$, and 8 orders as 5, 14, 8, and 1. This is consistent with the number of determinable parameters of 5, 15, 32, and 59 for $n = 2, 4, 6$, and 8 , as calculated from the difference between the total number of symmetry-allowed Hamiltonian terms of order n and the number of

Table 6Assignments^a, measured transition frequencies^b, and observed–calculated residuals^c from the fit for $m = 1, 2$, and ± 3 states.

Sym'	J'	Ka'	Kc'	Sym''	J''	Ka''	Kc''	Frequency MHz	o–c kHz
m = 1									
E1	3	2	2	E1	3	0	3	9262.3282(10)	6.2
E1	4	2	3	E1	4	0	4	10933.4502(5)	6.2
E1	5	2	4	E1	5	0	5	13585.9639(5)	–5.0
E1	6	2	5	E1	6	0	6	16888.9835(5)	–3.7
E1	7	2	6	E1	7	0	7	20452.0941(5)	–9.4
E1	8	2	7	E1	8	0	8	24054.7970(5)	–4.0
E2	2	1	2	E2	1	0	1	8480.8605(2)	–0.5
E1	3	0	3	E1	2	0	2	12399.1203(2)	–0.9
E1	4	0	4	E1	3	0	3	16004.8103(2)	1.5
E1	5	0	5	E1	4	0	4	19453.4022(5)	6.0
E1	6	0	6	E1	5	0	5	22877.8998(5)	2.9
E1	7	0	7	E1	6	0	6	26323.3065(5)	3.5
E2	4	1	3	E2	4	1	4	8955.1421(10)	–10.5
E2	5	1	4	E2	5	1	5	11995.8529(5)	0.1
E2	6	1	5	E2	6	1	6	15669.3021(5)	2.1
E2	7	1	6	E2	7	1	7	19596.7464(5)	–2.5
E2	8	1	7	E2	8	1	8	23516.9640(5)	–4.2
E2	3	1	3	E2	2	1	2	12292.1155(2)	1.3
E2	4	1	4	E2	3	1	3	15834.1902(2)	2.2
E2	5	1	5	E2	4	1	4	19301.7052(5)	5.6
E2	6	1	6	E2	5	1	5	22779.2947(5)	4.8
E2	7	1	7	E2	6	1	6	26268.4603(5)	4.2
E2	4	1	3	E2	3	1	2	17879.7694(2)	0.6
E2	5	1	4	E2	4	1	3	22342.4015(5)	1.7
E2	6	1	5	E2	5	1	4	26452.7376(5)	0.5
E2	2	2	1	E2	1	1	0	8584.3803(2)	–0.4
E1	3	2	2	E1	2	1	1	13103.3936(2)	–1.0
E1	2	1	1	E1	1	1	1	8613.5419(2)	–0.8
E2	3	2	1	E2	2	2	1	12930.5248(2)	–1.2
E1	4	2	3	E1	3	2	2	17675.9299(4)	–0.9
E1	5	2	4	E1	4	2	3	22105.9273(5)	6.2
E1	6	2	5	E1	5	2	4	26180.9212(5)	6.0
E1	5	2	3	E1	4	2	2	21957.8667(5)	5.2
E1	6	2	4	E1	5	2	3	26695.9192(5)	6.2
E1	3	3	1	E1	2	2	0	12894.2410(2)	–2.6
E2	4	3	2	E2	3	2	1	17344.1273(4)	–2.1
E1	6	2	4	E1	6	2	5	11606.8165(20)	0.7
E1	7	2	5	E1	7	2	6	13239.1058(10)	–2.2
E1	8	2	6	E1	8	2	7	16044.7996(50)	39.9
E1	9	2	7	E1	9	2	8	19712.6112(20)	–9.6
E1	10	2	8	E1	10	2	9	23809.9313(20)	–15.9
E2	9	3	6	E2	9	3	7	15946.2065(20)	–13.0
E2	10	3	7	E2	10	3	8	17105.9352(10)	9.0
E2	11	3	8	E2	11	3	9	19578.7349(10)	–7.8
E1	4	3	1	E1	3	3	1	17240.7550(4)	–2.3
E2	4	4	1	E2	3	3	0	17202.7294(4)	–3.9
E1	5	4	2	E1	4	3	1	21629.4650(5)	–1.4
E2	5	3	3	E2	4	3	2	21855.9046(5)	–1.4
E2	6	3	4	E2	5	3	3	26489.6701(5)	–0.5
E2	6	3	3	E2	5	3	2	26118.7716(5)	–1.1
E1	5	5	1	E1	4	4	0	21510.7065(5)	–5.3
E2	6	5	2	E2	5	4	1	25927.3926(5)	–6.3
E1	6	4	3	E1	5	4	2	26073.3138(5)	–0.6
E1	14	4	10	E1	14	4	11	22877.6780(50)	–20.1
E2	5	4	1	E2	4	4	1	21549.5355(5)	–2.8
E2	6	6	1	E2	5	5	0	25818.4078(5)	–10.8
E2	15	5	10	E2	15	5	11	24628.6842(20)	11.8
E1	6	5	1	E1	5	5	1	25857.7234(5)	–8.8
m = 2									
E1	4	0	4	E1	3	0	3	16650.3153(5)	4.5
E1	5	0	5	E1	4	0	4	20024.7641(5)	2.6
E1	6	0	6	E1	5	0	5	23276.7219(5)	0.5
E1	2	1	2	E1	1	0	1	8506.5453(5)	–4.3
E2	3	1	3	E2	2	0	2	12685.1587(5)	–0.7
E2	2	1	1	E2	1	1	1	8546.1911(5)	2.0
E1	3	1	2	E1	2	1	2	12843.5234(5)	3.6
E2	4	1	3	E2	3	1	3	18067.7461(5)	5.1
E1	2	2	1	E1	1	1	0	8558.4457(5)	1.0
E2	3	2	2	E2	2	1	1	12853.1851(5)	–1.2
E1	4	2	3	E1	3	1	2	17272.4147(5)	–1.1
E2	5	1	4	E2	4	1	3	22807.7538(5)	5.2
E2	5	1	4	E2	5	1	5	7980.2960(5)	16.0
E2	6	1	5	E2	6	1	6	12196.5462(10)	10.3

Table 6 (continued)

Sym'	J'	Ka'	Kc'	Sym''	J''	Ka''	Kc''	Frequency MHz	o–c kHz
E1	3	2	1	E1	2	2	1	12856.4233(5)	–3.1
E2	4	2	2	E2	3	2	2	17200.4659(5)	–1.4
E1	5	2	3	E1	4	2	3	21888.3302(5)	2.6
E2	3	3	1	E2	2	2	0	12857.8606(5)	1.0
E1	4	3	2	E1	3	2	1	17176.8127(5)	–4.9
E2	5	3	3	E2	4	2	2	21602.0872(5)	–1.9
E1	7	2	5	E1	7	2	6	8201.6323(10)	2.6
E1	8	2	6	E1	8	2	7	11720.0595(10)	7.8
E1	9	2	7	E1	9	2	8	16043.6560(20)	30.7
E1	6	2	4	E1	5	2	3	26835.8920(5)	3.8
E2	9	3	6	E2	9	3	7	8393.5233(10)	–1.8
E2	10	3	7	E2	10	3	8	10678.2165(10)	5.1
E1	4	4	1	E1	3	3	0	17160.2968(5)	–0.5
E2	5	4	2	E2	4	3	1	21493.4136(5)	–3.9
E1	6	4	3	E1	5	3	2	25915.0748(5)	–2.4
E2	4	3	1	E2	3	3	1	17166.1039(5)	–1.6
E1	5	3	2	E1	4	3	2	21527.0910(5)	–1.0
E2	6	3	3	E2	5	3	3	26076.8963(5)	–1.1
E2	5	5	1	E2	4	4	0	21464.2653(5)	1.8
E1	6	5	2	E1	5	4	1	25806.7500(5)	–1.4
E1	11	4	7	E1	11	4	8	9653.7309(10)	4.0
E1	12	4	8	E1	12	4	9	10446.0553(10)	–20.3
E1	13	4	9	E1	13	4	10	12575.8724(10)	–1.4
E1	5	4	1	E1	4	4	1	21475.2409(5)	–1.6
E2	6	4	2	E2	5	4	2	25844.6009(5)	–2.9
E2	6	5	1	E2	5	5	1	25783.9441(5)	–0.7
E1	6	6	1	E1	5	5	0	25769.0899(5)	0.0
E2	14	5	9	E2	14	5	10	11738.9981(10)	–0.6
E2	15	5	10	E2	15	5	11	12316.9362(10)	16.7
E2	16	5	11	E2	16	5	12	14168.9632(10)	–9.5
m = 3									
A1	20	1	19	A2	20	0	20	8566.7622(5)	1.2
A2	21	1	20	A1	21	0	21	9427.5950(10)	–3.6
A1	22	1	21	A2	22	0	22	10289.4040(10)	–1.7
A2	23	1	22	A1	23	0	23	11149.3240(10)	–3.0
A1	24	1	23	A2	24	0	24	12004.9952(10)	12.7
A2	25	1	24	A1	25	0	25	12854.3920(5)	0.0
A1	28	1	27	A2	28	0	28	15350.1059(10)	3.7
A2	2	1	1	A1	1	0	1	7967.0542(5) ^d	–2.9
B1	3	1	2	B2	2	0	2	12604.6570(5)	–0.9
A2	5	3	3	A1	5	0	5	9095.6028(10)	–2.6
B2	2	2	0	B1	1	1	0	8577.8119(5)	–1.9
A1	3	2	1	A2	2	1	1	12013.2625(5) ^d	–2.7
B2	4	2	2	B1	3	1	2	16787.3770(5)	–4.7
A1	5	2	3	A2	4	1	3	21558.8323(5)	0.0
B1	20	2	19	B2	20	1	20	8566.7622(5)	–3.0
B2	21	2	20	B1	21	1	21	9427.5950(10)	–5.4
B1	22	2	21	B2	22	1	22	10289.4040(10)	–2.5
B2	23	2	22	B1	23	1	23	11149.3240(10)	–3.3
B1	24	2	23	B2	24	1	24	12004.9952(10)	12.6
A1	2	2	1	A2	1	1	1	9086.8284(5) ^d	3.7
B2	3	2	2	B1	2	1	2	12779.7250(5)	–0.5
B2	5	2	4	B1	4	1	4	20787.3809(5)	–0.8
A1	7	3	4	A2	7	1	6	14726.7553(10)	–17.2
A1	5	2	3	A2	5	1	5	8907.1705(10)	9.2
A1	5	0	5	A2	4	1	3	12641.8804(10)	11.6
A2	6	3	3	A1	6	1	6	11348.4271(20)	–36.2
B2	17	3	14	B1	17	2	15	17230.2461(10)	–9.1
A1	12	4	9	A2	12	2	10	8283.8315(10)	0.6
A2	13	4	10	A1	13	2	11	10116.9392(10)	–2.3
A1	14	4	11	A2	14	2	12	11955.2468(10)	4.3
A2	15	4	12	A1	15	2	13	13768.4827(10)	6.4
A1	16	4	13	A2	16	2	14	15534.8515(10)	1.1
A2	3	3	1	A1	2	2	1	13685.1489(5) ^d	2.3
B1	4	3	2	B2	3	2	2	17212.9680(5)	1.2
A2	5	3	3	A1	4	2	3	21689.4823(5)	–2.3
B2	6	2	4	B1	6	2	5	9191.5159(10)	14.4
B1	7	2	5	B2	7	2	6	13508.8314(10)	9.9
B1	3	3	0	B2	2	2	0	12978.1748(5)	–0.2
B1	5	3	2	B2	4	2	2	20975.8900(5)	–1.5
B1	12	3	9	B2	12	3	10	8075.5276(10)	0.0
B2	13	3	10	B1	13	3	11	10002.1513(10)	1.4
B1	14	3	11	B2	14	3	12	11894.2178(10)	–1.9
B2	15	3	12	B1	15	3	13	13736.9888(10)	–1.0
B1	16	3	13	B2	16	3	14	15519.0073(10)	–12.3
B2	4	4	0	B1	3	3	0	17504.6262(5)	–2.6

Table 6 (continued)

Sym'	J'	Ka'	Kc'	Sym''	J''	Ka''	Kc''	Frequency MHz	o–c kHz
A1	5	4	1	A2	4	3	1	20404.0019(5) ^d	–0.9
B2	6	4	2	B1	5	3	2	25251.3970(5)	–3.1
A1	4	4	1	A2	3	3	1	18339.0350(5) ^d	1.6
B2	5	4	2	B1	4	3	2	21778.2628(5)	–2.6
B2	8	4	4	B1	8	3	5	11540.1694(10)	–24.2
B1	9	4	5	B2	9	3	6	12847.4094(10)	–3.9
B2	10	4	6	B1	10	3	7	15103.1536(10)	1.6
A2	17	4	14	A1	17	3	15	17238.0231(10)	–9.2
A2	19	4	16	A1	19	3	17	20405.6316(20)	–6.3
B1	7	5	2	B2	7	3	5	11707.2490(10)	–13.1
B1	7	5	2	B2	7	3	5	11707.2409(20)	–21.2
A1	8	5	3	A2	8	3	6	13393.5743(10)	–11.2
B1	10	6	5	B2	10	4	6	9495.9485(10)	–1.2
B2	11	6	6	B1	11	4	7	11119.4047(10)	2.6
B1	12	6	7	B2	12	4	8	12593.9917(10)	0.8
B2	13	6	8	B1	13	4	9	14043.0591(10)	12.1
B1	14	6	9	B2	14	4	10	15510.0435(10)	3.1
B2	15	6	10	B1	15	4	11	16931.0419(20)	2.6
A2	8	5	4	A1	8	4	5	10975.0034(10)	–16.6
A1	9	5	5	A2	9	4	6	13212.8309(10)	–10.8
A1	11	5	7	A2	11	4	8	18153.3049(10)	1.8
A2	14	5	10	A1	14	4	11	26035.0939(50)	–12.8
A2	5	5	1	A1	4	4	1	23052.7093(5) ^d	1.4
B1	6	5	2	B2	5	4	2	26506.2276(5)	–1.3
A2	6	5	1	A1	5	4	1	24852.0239(5) ^d	–0.3
A1	7	4	3	A2	7	4	4	9645.6970(10)	–10.8
A2	5	5	1	A1	5	4	1	8195.3487(10)	3.2
A1	12	5	7	A2	12	5	8	8593.0173(10)	–0.1
A2	13	5	8	A1	13	5	9	11326.6102(10)	2.6
A1	14	5	9	A2	14	5	10	13812.8818(10)	1.1
A2	15	5	10	A1	15	5	11	15945.1104(10)	–9.1
A2	8	6	2	A1	8	5	3	12121.0905(10)	6.7
A1	9	6	3	A2	9	5	4	11114.5309(10)	8.8
A2	10	6	4	A1	10	5	5	11193.2896(10)	8.3
A1	11	6	5	A2	11	5	6	12448.2405(10)	11.5
A2	12	6	6	A1	12	5	7	14660.7734(10)	–2.6
B1	23	6	17	B2	23	5	18	17175.1262(10)	–4.2
B1	29	6	23	B2	29	5	24	20814.0646(20)	–3.7
B2	19	6	14	B1	19	5	15	19614.5295(20)	–0.5
A1	6	6	1	A2	6	5	1	11165.8759(10)	6.4
B2	10	7	4	B1	10	6	5	10506.5090(10)	–8.0
B1	11	7	5	B2	11	6	6	10704.3338(10)	5.5
B2	12	7	6	B1	12	6	7	12245.1339(10)	0.5
A2	22	7	16	A1	22	6	17	14668.1114(10)	–7.4
A1	23	7	17	A2	23	6	18	17222.4604(10)	–7.0
B1	15	6	9	B2	15	6	10	21611.7102(20)	–0.5
B2	15	7	8	B1	15	6	9	8955.8813(10)	2.4
B1	16	7	9	B2	16	6	10	9143.3928(10)	8.8
A2	18	8	10	A1	18	7	11	8318.7513(10)	–7.1
A1	19	8	11	A2	19	7	12	11313.6324(10)	0.5
B1	21	8	13	B2	21	7	14	14581.6366(10)	1.2
A2	15	8	8	A1	15	7	9	14939.1531(20)	10.7
A2	20	8	13	A1	20	7	14	13100.4427(10)	3.7
A1	21	8	14	A2	21	7	15	13115.0151(10)	4.7
B2	23	9	14	B1	23	8	15	11721.5626(20)	–11.7
B2	23	9	14	B1	23	8	15	11721.5645(10)	–9.8
B1	24	9	15	B2	24	8	16	14536.9535(10)	–13.5
A1	15	8	7	A2	15	8	8	9369.0884(10)	10.2
B1	16	9	7	B2	16	9	8	10967.6945(10)	2.5
B2	17	9	8	B1	17	9	9	10237.8034(10)	4.8
B1	18	9	9	B2	18	9	10	12193.4994(10)	11.7
A1	22	10	13	A2	22	9	14	14203.6053(10)	20.9
m = –3									
B1	2	0	2	B2	1	0	1	8513.2174(5)	–8.2
B2	3	0	3	B1	2	0	2	12723.0622(5)	–3.1
B1	4	0	4	B2	3	0	3	16877.7193(5)	–2.8
B2	5	0	5	B1	4	0	4	20961.6418(5)	–1.6
B1	6	0	6	B2	5	0	5	24963.9204(5)	–0.6
A2	2	1	1	A1	1	1	0	9097.4572(5) ^d	0.3
A1	3	1	2	A2	2	1	1	13632.9094(5) ^d	–1.1

Table 6 (continued)

Sym'	J'	Ka'	Kc'	Sym''	J''	Ka''	Kc''	Frequency MHz	o–c kHz
A2	4	1	3	A1	3	1	2	18151.0691(5) ^d	2.4
A1	5	1	4	A2	4	1	3	22643.9567(5) ^d	0.5
A1	2	1	2	A2	1	1	1	7977.7921(5) ^d	4.3
A2	3	1	3	A1	2	1	2	11954.9221(5) ^d	–3.7
A1	4	1	4	A2	3	1	3	15919.4783(5) ^d	–2.5
A2	5	1	5	A1	4	1	4	19869.8834(5) ^d	–1.9
A1	6	1	6	A2	5	1	5	23807.0282(5) ^d	–2.7
A1	5	1	4	A2	5	1	5	8363.2376(10)	–4.3
A2	6	1	5	A1	6	1	6	11658.1096(10)	13.9
B1	10	2	8	B2	10	2	9	8473.2851(10)	–13.2
B2	11	2	9	B1	11	2	10	11610.0573(10)	1.0
B1	3	2	2	B2	2	2	1	12812.8261(5)	4.3
B2	4	2	3	B1	3	2	2	17063.1099(5)	0.5
B1	5	2	4	B2	4	2	3	21295.8534(5)	–0.1
B2	6	2	5	B1	5	2	4	25507.0299(5)	0.1
B2	3	2	1	B1	2	2	0	12892.0270(5)	2.5
B1	4	2	2	B2	3	2	1	17260.0325(5)	–3.8
B2	5	2	3	B1	4	2	2	21685.4289(5)	1.9
B1	6	2	4	B2	5	2	3	26175.9618(5)	0.4
A2	4	3	1	A1	3	3	0	17144.8780(5)	0.9
A1	5	3	2	A2	4	3	1	21456.0109(5)	5.5
A2	6	3	3	A1	5	3	2	25787.6472(5)	0.2
A1	4	3	2	A2	3	3	1	17140.6250(5)	3.0
A2	5	3	3	A1	4	3	2	21441.1666(5)	2.3
A1	6	3	4	A2	5	3	3	25748.3042(5)	–1.9
A1	15	3	12	A2	15	3	13	9789.6866(10)	1.2
A2	16	3	13	A1	16	3	14	13169.6608(10)	–5.3
A1	17	3	14	A2	17	3	15	17084.4930(10)	7.0
A2	18	3	15	A1	18	3	16	21418.8830(10)	–0.9
A1	19	3	16	A2	19	3	17	25984.0791(10)	7.2
B1	5	4	2	B2	4	4	1	21439.5091(5)	6.2
B2	6	4	3	B1	5	4	2	25747.1714(5)	2.9
B2	19	4	15	B1	19	4	16	9032.6251(10)	–5.8
B1	20	4	16	B2	20	4	17	12273.9621(10)	2.4
B2	5	4	1	B1	4	4	0	21439.7281(5)	1.3
A1	23	5	18	A2	23	5	19	8865.3682(10)	–3.8
A2	24	5	19	A1	24	5	20	12076.3057(10)	–1.2
A1	6	5	2	A2	5	5	1	25739.3154(5)	11.7
A2	6	5	1	A1	5	5	0	25739.3154(5)	–0.2
m = –3 ← +3									
A1	22	0	22	A2	22	4	18	15970.8547(10)	5.4
A2	23	0	23	A1	23	4	19	13852.9884(10)	6.1
A1	24	0	24	A2	24	4	20	11479.6572(10)	7.6
A2	25	0	25	A1	25	4	21	8956.5853(10)	13.4
B1	22	1	22	B2	22	5	18	15973.7345(10)	–4.6
B2	23	1	23	B1	23	5	19	13853.8788(10)	–6.4
B1	24	1	24	B2	24	5	20	11479.8750(10)	–15.7
B2	25	1	25	B1	25	5	21	8956.5853(10)	–29.1
A1	16	0	16	A2	16	7	10	11579.2446(10)	6.1
A2	22	1	21	A1	22	7	15	11251.3890(10)	10.9
A1	23	1	22	A2	23	7	16	8012.4732(10)	11.0
B1	26	2	24	B2	26	8	18	15458.6873(20)	15.8
B2	27	2	25	B1	27	8	19	13792.2804(10)	–16.8
B1	28	2	26	B2	28	8	20	11169.2181(20)	0.5
B2	22	2	21	B1	22	8	15	11726.6687(20)	8.1
B1	23	2	22	B2	23	8	16	8088.9963(10)	19.8
A2	27	3	25	A1	27	9	19	14043.9061(10)	0.6
A1	28	3	26	A2	28	9	20	11241.2957(10)	14.1
A2	29	3	27	A1	29	9	21	7974.5918(20)	–4.5
A1	27	3	24	A2	27	12	15	10526.6805(10)	–13.6
m = +3 ← –3									
A1	21	6	15	A2	21	1	20	11438.4671(10)	–10.5
A1	28	7	21	A2	28	1	27	11126.1558(10)	12.0
B1	21	6	16	B2	21	1	21	11281.9545(50)	–8.0
B2	16	9	8	B1	16	1	16	10564.4233(10)	6.1
A1	18	11	7	A2	18	1	17	8124.3007(10)	14.1
A2	19	11	8	A1	19	1	18	14479.9208(50)	46.5
B2	22	12	11	B1	22	2	20	9669.2884(10)	–6.9
A2	21	10	12	A1	21	2	20	10052.9627(10)	–0.3
B1	28	8	21	B2	28	2	27	11141.5703(10)	3.2

(continued on next page)

Table 6 (continued)

Sym'	J'	Ka'	Kc'	Sym''	J''	Ka''	Kc''	Frequency MHz	o-c kHz
B2	29	8	22	B1	29	2	28	14012.7732(10)	7.5
B2	26	11	16	B1	26	3	24	11167.1221(10)	-6.2
B1	29	14	16	B2	29	4	25	10964.8262(10)	-1.7
A1	30	12	19	A2	30	4	27	8732.9536(10)	-3.7

^a The eight assignment columns give the upper state (') torsion-rotation symmetry in G_{12} , and J , K_a , K_c rotational quantum numbers followed by the same quantities for the lower state ('').

^b The measurements are given in MHz; their uncertainties are given in kHz in parentheses. Measurements for $m = 0$ transitions can be found in [11].

^c The o-c values are residuals in kHz from our final least squares fit. The full fit is given in Table S1 of the electronic supplementary information.

^d The $m = \pm 3$, $K = \pm 1$ doublet lines of the type that were used in [8] for barrier determination from their splitting. Note that $m = -3$ lines of this type have traditional K_a labels (essentially because $m = -3$ levels with $J = K$ in Fig. 2 increase monotonically in energy, similar to $m = 0$), but that $m = +3$ lines of this type are given non-traditional K_a values by the labeling algorithm of the program (see text).

symmetry-allowed contact transformation terms of order $n-1$ [33].

There is a correlation problem involving the F and ρ parameters that should be discussed in connection with Table 8. Initially the parameter ρ was treated in the fit as an adjustable parameter. (This is the way the ρ parameter is treated in BELGI [19,20].) Nevertheless in our final fit we decided to use the form shown in Table 8, where the $F(P_x - \rho P_a)^2 + AP_a^2$ part of Eq. (10) is regrouped as

Table 7

Summary of the least squares fit.

Organized by torsional state					Organized by measurement precision			
m^a	m'^a	# ^b	J_{max}^c	rms ^d	unc ^e	# ^f	J_{max}^c	rms ^d
0	0	91	30	3.7	2	26	5	1.5
1	1	58	15	8.0	4	6	5	3.1
2	2	44	16	7.4	5	169	30	3.4
-3	-3	46	24	4.6	10	147	30	8.3
+3	+3	107	29	8.3	20	19	29	14.5
± 3	∓ 3	33	30	13.5	50	5	21	29.6

^a Upper and lower state free-rotor quantum number m .

^b The number of transitions in a given category. The total number of transitions is 379, some of which are blended.

^c The maximum J in a given category.

^d The root-mean-square obs-calc residual for a given category in kHz. The overall rms is 7.4 kHz and the overall weighted rms is 0.75.

^e The assigned measurement precision for a given category in kHz.

^f The number of measured lines in each category. Some of the lines correspond to blended transitions. The total number of different line frequencies is 372.

$FP_x^2 + (A + \rho^2 F)P_a^2 - 2F\rho P_x P_a$, with the corresponding fitted parameters in the program being $B_{0000200} = F$, $B_{0100100} = -2F\rho$ and $B_{0200000} = A_{eff} - 1/2(B + C)$, instead of F , ρ and $A - 1/2(B + C)$. The two forms give an identical root-mean-square (rms) deviation of the fit, but the regrouped constants are less correlated, i.e., when F , ρ and $A - 1/2(B + C)$ are floated, F and ρ are highly correlated with each other (correlation coefficient -0.9997) as well as both

Table 8

Fitted parameters from the toluene $|m| \leq 3$ data set.

ntr^a	Operator ^b	Parameter ^{b,c}	Value ^{b,d} (cm ⁻¹)	Eq. (4) term ^e
220	P_x^2	F	5.466956(51)	$B_{0000200}$
211	$P_x P_a$	$-2\rho F$	-0.379765511(92)	$B_{0100100}$
202	P_a^2	$A_{eff} - (1/2)(B + C)$	0.1199611083(65)	$B_{0200000}$
	P^2	$(1/2)(B + C)$	0.0711555699(17)	$B_{1000000}$
	$P_b^2 - P_c^2$	$(1/2)(B - C)$	0.01281837326(83)	$B_{0020000} - B_{0002000}$
440	$(1/2)(1 + \cos 6\alpha)$	V_6	4.83783617(94)	$(1/2)(B_{0000000} + B_{0000020})$
431	$P_x^3 P_a$	ρ_m	$0.07238(11) \times 10^{-3}$	$B_{0100300}$
	$(1/2)\{P_x \sin 3\alpha\} P_c$	ρ_{3c}	$-8.5536(26) \times 10^{-3}$	$B_{0001101}$
422	$P_x^2 P^2$	F_j	$-0.3677(13) \times 10^{-6}$	$B_{1000200}$
	$P_x^2 P_a^2$	F_K	$-3.592(27) \times 10^{-6}$	$B_{0200200}$
	$(1/2)(P_a P_b + P_b P_a) \cos 3\alpha$	D_{3ab}	$0.2048(18) \times 10^{-3}$	$B_{0110010}$
413	$P_x P_a P^2$	ρ_j	$0.11250(16) \times 10^{-6}$	$B_{1100100}$
	$P_x P_a^3$	ρ_K	$0.1279(43) \times 10^{-6}$	$B_{0300100}$
	$(1/2)\{P_a, (P_b^2 - P_c^2)\} P_x$	ρ_{bc}	$0.05124(18) \times 10^{-6}$	$B_{0120100} - B_{0102100}$
404	$-P^4$	Δ_j	$0.0041957(98) \times 10^{-6}$	$-B_{2000000}$
	$-P^2 P_a^2$	Δ_{JK}	$0.012096(71) \times 10^{-6}$	$-B_{1200000}$
	$-P_a^4$	Δ_K	$0.02647(22) \times 10^{-6}$	$-B_{0400000}$
	$-2P^2(P_b^2 - P_c^2)$	δ_j	$0.0013451(28) \times 10^{-6}$	$-2(B_{1020000} - B_{1002000})$
	$-(P_a^2, (P_b^2 - P_c^2))$	δ_K	$0.014971(44) \times 10^{-6}$	$-2(B_{0220000} - B_{0202000})$
651	$P_x^5 P_a$	ρ_{mm}	$2.268(11) \times 10^{-6}$	$B_{0100500}$
642	$P_x^4 P_a^2$	F_{mK}	$-0.1848(30) \times 10^{-6}$	$B_{0200400}$
	$P_x^4 P^2$	F_{mj}	$0.00198(14) \times 10^{-6}$	$B_{1000400}$
	$P^2 \cos 6\alpha$	V_{6j}	$-5.5186(11) \times 10^{-6}$	$B_{1000020}$
	$(1/2)(P_b P_c + P_c P_b) \sin 6\alpha$	D_{6bc}	$8.6517(68) \times 10^{-6}$	$B_{0011002}$
633	$P_x^3 P_a^3$	ρ_{mK}	$0.0330(18) \times 10^{-6}$	$B_{0300300}$
624	$P_x^2 P_a^4$	F_{KK}	$-1.036(54) \times 10^{-9}$	$B_{0400200}$
	$P_x^2 P^2 P_a^2$	F_{JK}	$0.1244(81) \times 10^{-9}$	$B_{1200200}$
853	$P_x^3 P_a^3$	ρ_{mmK}	$-1.97(16) \times 10^{-9}$	$B_{0300500}$

^a $n = t + r$, where n is the total order of the operator, t is the order of the torsional part and r is the order of the rotational part, respectively.

^b $\{A, B\} = AB + BA$. The product of the operator in the second column of a given row and the parameter in the third column of that row gives the term actually used in the torsion-rotation Hamiltonian of the program. The numerical value of the parameter determined in the present least squares fit is given in the fourth column of that row.

^c Parameter nomenclature based on the subscript procedures of [32]. Note, however, that a few higher-order parameters differ by a factor of 2 from Table 2 of [32] to simplify their correspondence to the coefficients B_{kmqrst} in the Hamiltonian of Eq. (4).

^d All values are in cm⁻¹. Statistical uncertainties are shown as one standard uncertainty in the last two digits, type A, $k = 1$ in the notation of [36].

^e This column is included as an aid to the reader in understanding how the terms of the Hamiltonian are coded in the program. If each B_{kmqrst} coefficient in this column is multiplied by its appropriate partner expression from Eq. (4) and then artificially set to +1.0, the operator in column 2 is obtained.

Table 9
Comparison of selected fitted parameters with previous results.

Parameter	This work	Previous work	Refs.
V_6 (cm ⁻¹)	4.83783617(94)	4.88(3)	[8]
V_6 (cal mol ⁻¹)	13.8320679(27)	13.94(10)	[8]
F (MHz)	163895.2(15)	166726.46 ^a	[8]
ρ	0.03473281(32)	0.03436362 ^b	[8]
$A_{\text{eff}} = A + F\rho^2$ (MHz)	5729.53387(21)	5729.47685(22)	[11]
B (MHz)	2517.475482(57)	2517.478322(52)	[11]
C (MHz)	1748.905156(56)	1748.856375(43)	[11]
Δ_J (kHz)	0.12578(29)	0.125438(14)	[11]
Δ_{JK} (kHz)	0.3626(21)	0.37914(58)	[11]
Δ_K (kHz)	0.7935(65)	0.8101(27)	[11]
δ_J (kHz)	0.040324(85)	0.0401403(48)	[11]
δ_K (kHz)	0.4488(13)	0.44741(17)	[11]

^a Calculated in [8] from an assumed value of $I_x = 3.14 \text{ u}\text{\AA}^2$.

^b Given by I_x/I_a , where $I_a = I'_a + I_x$, and I'_a results from $A' = 5729.325(60)$ MHz fitted in [8].

being correlated with $A - (1/2)(B + C)$ (correlation coefficients ± 0.994). No large correlation between the $B_{0000200}$, $B_{0100100}$ and $B_{0200000}$ parameters is observed in the regrouped case.

In Table 9 we compare some of our parameters with previously determined values [8,11]. The presently determined height of the sixfold barrier, $V_6 = 4.8378362(9) \text{ cm}^{-1}$, is in good agreement with $V_6 = 4.88(3) \text{ cm}^{-1}$ determined by Rudolf et al. [8]. The 33 transitions of the $m = +3 \leftrightarrow m = -3$ type that were measured and fit in the present study add considerably more confidence to the V_6 value, since the gap between $m = +3$ and $m = -3$ states is known to be directly connected to the height of the sixfold potential barrier. This is a rather different situation from that in [8] where the splitting in two pairs of $J = 3 \leftarrow 2$, $|m| = 3$, $|K| = 1$ transitions constituted the basis for evaluation of V_6 . Even though transitions of this type are no longer the sole basis for the determination of V_6 we have also considerably extended measurements of such transition pairs, and remeasured the four transitions from [8] at the greater precision offered by the waveguide FTMW spectrometer used in the present study. The pertinent transitions are identified in Table 6 and are also listed separately in Table S2. We note finally that a number of very different exploratory fits of the present data set gave V_6 values that were stable at the level of 10^{-5} cal/mol, even though the F values from these fits differed by as much as 8%. We hope that addition of transitions with higher m values (see below) will give an F value that is as stable as the present V_6 value.

The values of A_{eff} , B , C , and the quartic centrifugal distortion constants are in good agreement with those from the recent $m = 0$ study [11]. The level of the current understanding of the lower- J room-temperature spectrum of toluene is illustrated in Fig. 3. All R -type transitions in the plotted spectra are accounted for up to $|m| = 5$, even though the current fit is up to $|m| \leq 3$. All but the two strongest lines in the $J = 2 \leftarrow 1$ region appear to follow an approximate intensity profile consisting of two free-rotation type wings, one to low- and the second to high-frequency from the free-rotation band center at $2(B + C) = 8532.7$ MHz (see Fig. 12.14 of [34] for an oblate top case). In the $J = 3 \leftarrow 2$ region there is a much larger number of strong lines to high-frequency from the corresponding band center at $3(B + C) = 12799.1$ MHz, although there is a discernible clustering of unassigned $|m| > 5$ lines around this frequency.

It is also of considerable interest to discuss the $\cos 3\alpha$ and $\sin 3\alpha$ structural relaxation terms determined in our study and the possibility of determining the sign of the V_6 potential term from microwave data alone. Although our fit of the current data set does indeed prefer the plus sign in the sixfold potential function, the difference between fits with plus and minus signs is not very pronounced. The fit with a plus sign gives an rms deviation of 7.4 kHz, whereas the fit with a minus sign gives an rms deviation of 8.9 kHz. Moreover, if several $m = 2$ Q -type transitions from the region where $m = 1$ and $m = 2$ levels start to overlap are excluded, then a fit without any $\cos 3\alpha$ or $\sin 3\alpha$ relaxation terms at all can be obtained with only a slightly larger rms deviation of 9.9 kHz, meaning that these structural relaxation terms are only marginally important for the current dataset. The explanation for this fact presumably lies in the relative lack of $\Delta m \neq 0$ interactions in the current data set. From the point of view of the Hamiltonian matrix, the $\cos 3\alpha$ and $\sin 3\alpha$ relaxation terms appear as $\Delta K = 1$ interaction terms between different m states, and it is expected that these terms will be most important in the region with overlapping energy levels from $|m| = 1$ and $|m| = 2$. (Sørensen and Pedersen had numerous transitions involving levels in such overlap regions when they determined the sign of V_6 in their nitromethane study [3]). In our current dataset only a few $m = 2$, Q -type transitions fall in the region with overlapping $|m| = 1$ and $|m| = 2$ energy levels, and probably many more transitions from this region will have to be included in the fit before we can see striking differences between fits with the plus and minus sign choice in the potential function.

Summarizing this issue we can say that the present microwave data set does not allow a determination of the sign of the V_6 potential function with good confidence from the rms deviation of the fit.

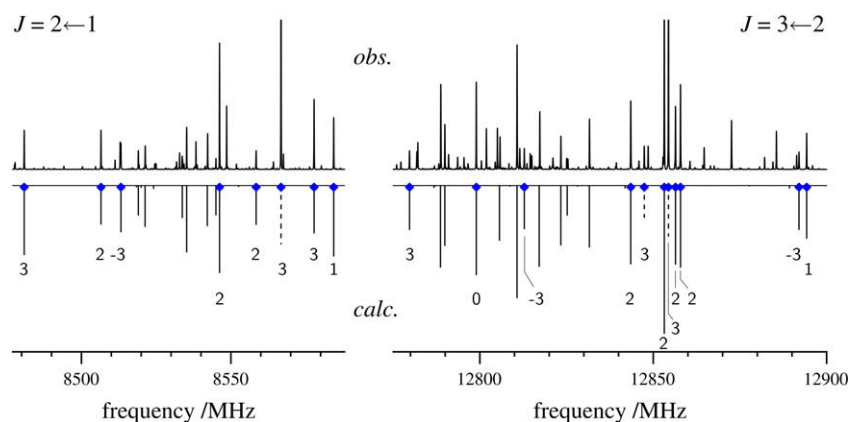


Fig. 3. Comparison of the observed room-temperature rotational spectrum of toluene in the vicinity of two successive low- J bandheads of R -type transitions with a calculation from the current fit. Dashed lines indicate assigned Q -type transitions falling in these regions and the diamond symbols mark lines that are in the current fit. Values of m are marked for all transitions with $|m| \leq 3$. The remaining strong lines in the prediction are for $|m| = 4$ and 5 and are seen to have clear counterparts in the spectrum, although $|m| \geq 4$ transitions are outside the scope of the present stage of the analysis.

Nevertheless, the sign of V_6 preferred by our current fit, which corresponds to the equilibrium configuration in which one hydrogen atom of the methyl top is perpendicular to the plane of the phenyl ring, rather than lying in the plane of the ring, is in agreement with *ab initio* calculations [6,35] as well as with the results of an S_1-S_0 fluorescence study of toluene [7]. We hope that expansion of our data set to higher J will allow us to make a more definitive statement on the sign of V_6 obtained from microwave data only.

In the future we plan to test the model and the program further by including toluene transitions involving higher values of $|m|$ and J in our fits. For the purpose of going up smoothly in J assignments, we plan to supplement the presently available data set by measurements in the 50–150 GHz range, which will fill the gap in current coverage. Also there are still many lines in the available records which remain unassigned, some of which certainly correspond to higher $|m|$ and J transitions.

In conclusion, the present fit is the first fit to experimental accuracy of a rather extensive data set of $|m| \leq 3$ transitions in toluene. This fit can also be taken as a demonstration of the correctness of the new program on the example molecule toluene.

Acknowledgments

Dr. Sergei Tashkun is gratefully acknowledged for fruitful discussions on the band matrix diagonalization problem and providing a copy of the SBR package. We also thank Dr. Isabelle Kleiner for numerous helpful discussions concerning procedures in her program BELGI. The Warsaw authors acknowledge financial support from the Polish Ministry of Science and Higher Education, Grant No. N-N202-0541-33.

Appendix A. Supplementary data

Supplementary data associated with this article can be found, in the online version, at doi:10.1016/j.jms.2009.10.005.

References

- [1] E.B. Wilson Jr., C.C. Lin, D.R. Lide Jr., *J. Chem. Phys.* 23 (1955) 136–142.
- [2] H.C. Longuet-Higgins, *Mol. Phys.* 6 (1963) 445–460.

- [3] G.O. Sørensen, T. Pedersen, *Studies in Physical and Theoretical Chemistry*, vol. 23, Elsevier, 1983, pp. 219–236.
- [4] T.J. Sears, P.M. Johnson, P. Jin, S. Oatis, *J. Chem. Phys.* 104 (1996) 781–792.
- [5] X.-Q. Tan, D.W. Pratt, *J. Chem. Phys.* 100 (1994) 7061–7067.
- [6] A.L.L. East, H. Liu, E.C. Lim, P. Jensen, I. Déchéne, M.Z. Zgierski, W. Siebrand, P.R. Bunker, *J. Chem. Phys.* 112 (2000) 167–175.
- [7] D.R. Borst, D.W. Pratt, *J. Chem. Phys.* 113 (2000) 3658–3669.
- [8] H.D. Rudolph, H. Dreizler, A. Jaeschke, P. Wendling, *Z. Naturforsch.* 22a (1967) 940–944.
- [9] W.A. Kreiner, H.D. Rudolph, B.T. Tan, *J. Mol. Spectrosc.* 48 (1973) 86–99.
- [10] V. Amir-Ebrahimi, A. Choplin, J. Demaison, G. Roussy, *J. Mol. Spectrosc.* 89 (1981) 42–52.
- [11] Z. Kisiel, E. Białkowska-Jaworska, L. Pszczółkowski, H. Mäder, *J. Mol. Spectrosc.* 227 (2004) 109–113.
- [12] H. Hartwig, H. Dreizler, *Z. Naturforsch.* 51a (1996) 923–932.
- [13] H.M. Pickett, *J. Mol. Spectrosc.* 148 (1991) 371–377.
- [14] H.M. Pickett, SPFIT/SPCAT package. Available from: <<http://spec.jpl.nasa.gov>>.
- [15] P.R. Bunker, P. Jensen, *Molecular Symmetry and Spectroscopy*, NRC Research Press, Ottawa, 1998.
- [16] J.T. Hougen, *J. Mol. Spectrosc.* 256 (2009) 170–185.
- [17] G. Herzberg, *Infrared and Raman Spectra of Polyatomic Molecules*, Van Nostrand, New Jersey, 1945.
- [18] E. Herbst, J.K. Messer, F.C. De Lucia, P. Helminger, *J. Mol. Spectrosc.* 108 (1984) 42–57.
- [19] I. Kleiner, M. Godefroid, M. Herman, A.R.W. McKellar, *J. Mol. Spectrosc.* 142 (1990) 238–253.
- [20] Z. Kisiel, “PROSPE – Programs for ROTational SPEctroscopy” website. Available from: <<http://info.ifpan.edu.pl/~kisiel/prospe.htm>>.
- [21] V. Ilyushin, E. Alekseev, J. Demaison, I. Kleiner, *J. Mol. Spectrosc.* 240 (2006) 127–132.
- [22] C.H. Bischof, B. Lang, X. Sun, *ACM Trans. Math. Software* 26 (2000) 602–616.
- [23] Available from: <<http://www.netlib.org/lapack/>>.
- [24] M. Krüger, H. Dreizler, *Z. Naturforsch.* A 45 (1990) 724–726.
- [25] M. Krüger, H. Harder, C. Gerke, H. Dreizler, *Z. Naturforsch.* A 48 (1993) 737–738.
- [26] V. Meyer, W. Jäger, R. Schwarz, H. Dreizler, *Z. Naturforsch.* A 46 (1991) 445–449.
- [27] Z. Kisiel, J. Kosarzewski, L. Pszczółkowski, *Acta Phys. Pol.* A 92 (1997) 507–516.
- [28] C.C. Lin, J.D. Swalen, *Rev. Mod. Phys.* 31 (1959) 841–892.
- [29] I. Kleiner, J.T. Hougen, J.-U. Grabow, S.P. Belov, M. Yu. Tretyakov, J. Cosléou, *J. Mol. Spectrosc.* 179 (1996) 41–60.
- [30] M.A. Mekhtiev, J.T. Hougen, *J. Mol. Spectrosc.* 187 (1998) 49–60.
- [31] W.G. Harter, C.W. Patterson, *J. Chem. Phys.* 80 (1984) 4241–4261.
- [32] Li-Hong Xu, J. Fisher, R.M. Lees, H.Y. Shi, J.T. Hougen, J.C. Pearson, B.J. Drouin, G.A. Blake, R. Braakman, *J. Mol. Spectrosc.* 251 (2008) 305–313.
- [33] K. Nakagawa, S. Tsunekawa, T. Kojima, *J. Mol. Spectrosc.* 126 (1987) 329–340.
- [34] W. Gordy, R.L. Cook, *Microwave Molecular Spectra*, Wiley, New York, 1984.
- [35] K.-T. Lu, F. Weinhold, J.C. Weisshaar, *J. Chem. Phys.* 102 (1995) 6787–6805.
- [36] B.N. Taylor, C.E. Kuyatt, NIST Technical Note No. 1297 (1994). Available from: <<http://physics.nist.gov/Pubs/guidelines/contents.html>>.